CHAPTER V
COLUMN ANALYSIS

In this chapter, the moment-curvature and lateral force-displacement analysis of monolithic and precast columns are presented

5.1 Description of column analyzed

The properties of the column are based on the standarad drawings of the Road Department of Thailand. The model column is a 400x400 mm^2 square column. The section consists of 12DB20-SD50 longitudinal bars and RB9@100mm square hoops at the middle and bottom parts. This column used as the monolithic column. For the precast column with mechanical splices, the splice shows in Figure 5.1 are used. The buckling length is 200 mm according to the prediction by Dhakal (2002). That buckling length obtained from the second mode of buckling and has the value equal to 2 times the tie spacing. The calculation procedure for the buckling length is discussed in detail in Chapter 3. The total axial load for one column is 341 KN. The concrete strength at 28 days is 25 MPa. Figure 5.2 shows details of the column.

The AASHTO Standard Specifications (2002) for column reinforcement in seismic zone regarding the tie spacing for confinement are considered. Table 5.1 summarizes the properties of typical column section.

Figure 5.1 Typical mechanical splice selected for the section analysis

Table 5.1 Sectional properties of the column

Section type	Value	Remark
Column height (m)	3	
Section width (m)	0.4	
Effective depth (m)	0.346	
Gross section area (m2)	0.16	
Moment of inertia (m4)	0.00213	
Radius of gyration (m)	0.115	
Slenderness ratio	26.09	
Axial load ratio (Nu/fc'Ag)	0.087	
Concrete cover (m)	0.035	
Concrete strength (MPa)	25.0	
Longitudinal reinforcement ratio (%)	2.36	
Volumetric ratio (%)	0.77	
Maximum moment capacity (MN.m)	0.3211	
Shear force (MN)	0.107	
Concrete shear strength (MN)	0.132	
Lateral reinforcement shear strength (MN)	0.104	
Shear ratio	0.154	
Shear force/Shear strength	0.458	Flexural failure mode

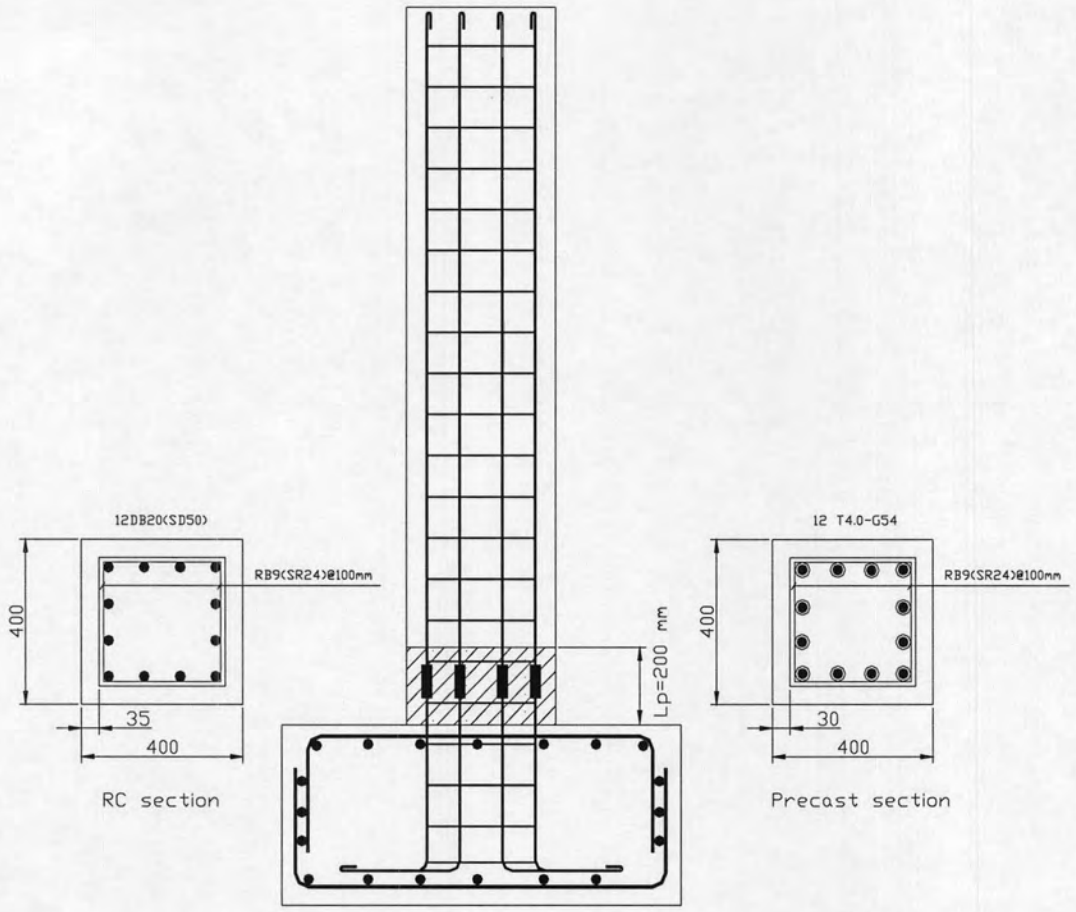

Figure5.2 Typical column properties for this study

In order to be apply the material behavior of the mechanical splices in section analysis, the average stresses are computed by dividing the actual load to the bar area as shown in Figure 5.3. The average strain is determined by solving for the ratio of the total deformation of the mechanical splice and the total gauge length. Finally, the average stress-strain relation was obtained in Figure 5.4.

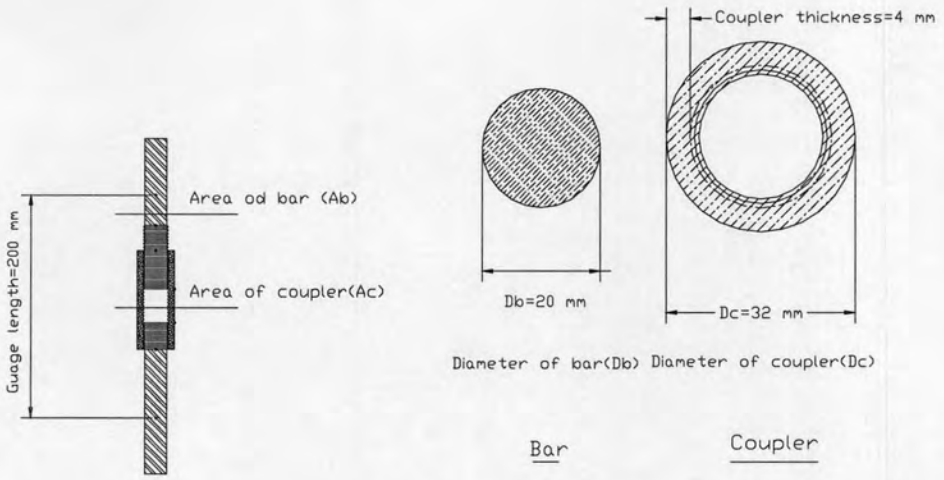

(a) Average gauge length and area (b) Bar and coupler sections

Fig 5.3 Sectional properties of the bar and coupler with thickness equal to 4.0 mm

Table 5.2: Sectional properties of bar and coupler (t = 4.0 mm)

Section	Diameter	Area	Moment of inertia
	(mm)	(mm^2)	(mm^4)
Bar	20	314.16	7854.00
Coupler (T4.0)	32	353.50	79765.35

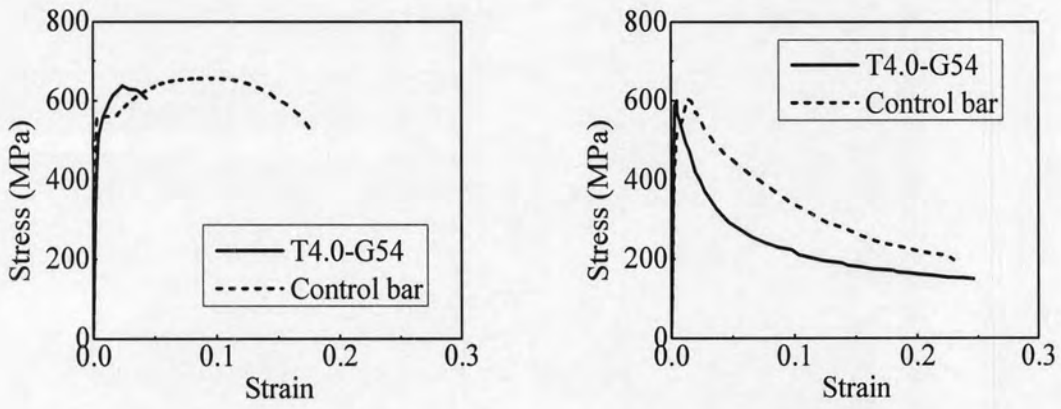

(a) Tension (b) Compression

Figure 5.4 Average stress-strain curves of control bar and mechanical splice T4.0-G54

5.2 Moment-curvature analysis of the RC and precast column sections

To obtain the theoretical moment-curvature relationship for a given section with flexure and axial load, the strain in the extreme compression fiber ε_c is incremented. For each value of ε_c the neutral axis position is determined by an interative process to make the sum of the internal forces determined from the strain profile equal to the external axial load. The moment and curvature corresponding to that particular concrete strain ε_c can then be determined.

In this research, assumptions are as follows:

1) The longitudinal strain in the steel and concrete at the various section levels is directly proportional to the distance from the neutral axis.

2) The tensile stress-strain curve for the steel has the general shape including strain hardening as shown in Figure 5.5.The compressive stress-strain curve is also including strain softening. All curves were obtained from the experiment.

3) The tensile stress of concrete is neglected

4) The unconfined concrete model of Kent and Park (1971) is applied for covering concrete. It is assumed that the cover concrete with a strain greater than 0.004 spalls and does not carry any stress.

5) The confined concrete model of Hoshkuma et al (1997) is applied for the core concrete. The sustained stress after the falling branch assumed equal to 20% of the peak stress. This is referred from Kent and Park (1971), Fuji et al. (1988); Sattcioglu and Razvi (1992). The model is shown in Figure 5.7

6) The maximum moment is defined as the greatest moment and the ultimate moment is defined as the moment dropped by 20% from the peak moment or the splice fracture.

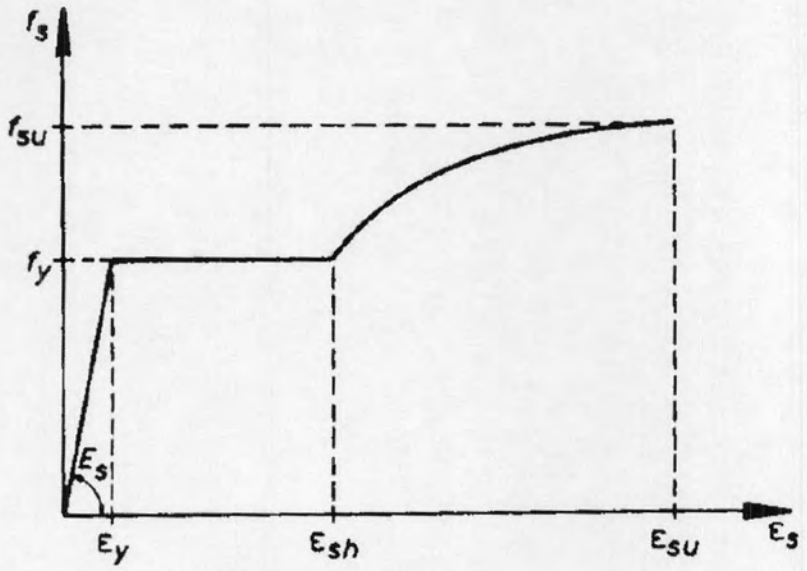

Figure 5.5 Tensile stress-strain model of reinforcing steel

5.2.1 Concrete models

1) Unconfined concrete model

The unconfined concrete model of Kent and Park (1971) applied for the covering concrete . The stress-strain relation illustrates in Figure 5.6.

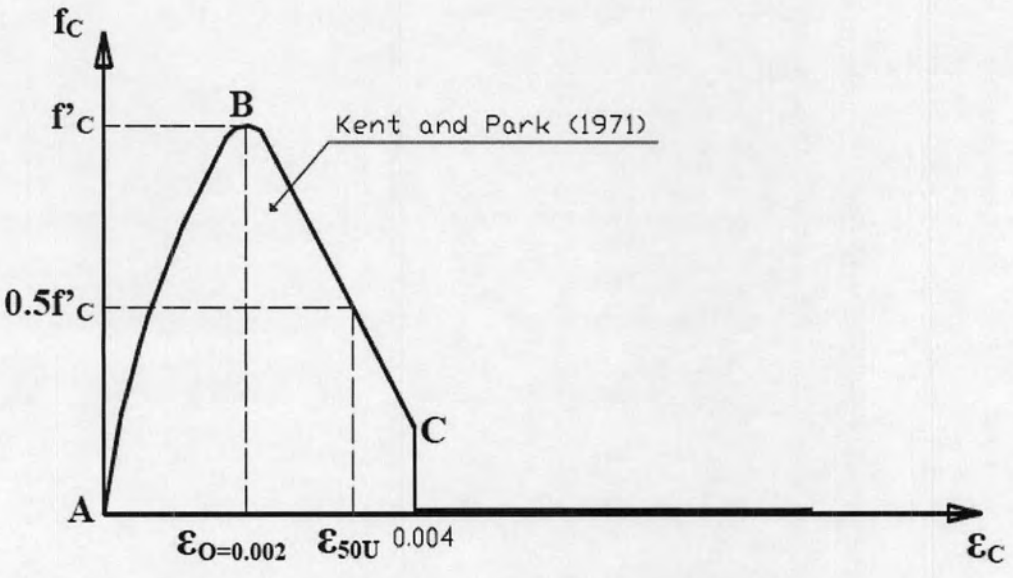

Figure 5.6 Unconfined concrete model by Kent and Park (1971)

From A-B ($\varepsilon_c \leq \varepsilon_o$):

$$f_c = f_c' \left[\frac{2\varepsilon_c}{\varepsilon_o} - \left(\frac{\varepsilon_c}{\varepsilon_o} \right)^2 \right] \tag{5.1}$$

From B-C ($\varepsilon_c > \varepsilon_o$):

$$f_c = f_c' - Z_1(\varepsilon_c - \varepsilon_o) \qquad \text{When, } \varepsilon_c < 0.004 \tag{5.2a}$$

$$f_c = 0 \qquad \text{When, } \varepsilon_c \geq 0.004 \tag{5.2b}$$

where

$$Z_1 = \frac{0.5f_c'}{\varepsilon_{50u} - 0.002} \tag{5.3a}$$

$$\varepsilon_{50u} = \frac{3 + 0.002f_c'}{f_c' - 1000} \tag{5.3b}$$

ε_0 = strain at ultimate stress of concrete (0.002)

f_c' = specified compressive strength of concrete. Use (MPa) for equation (5.1) to (5.2a) and use (psi) for equation (5.3b).

2) Confined concrete model

The confined concrete of Hoshikuma *et al.* (1997) applied for the core concrete. The stress-strain relation depicted in Figure 5.7:

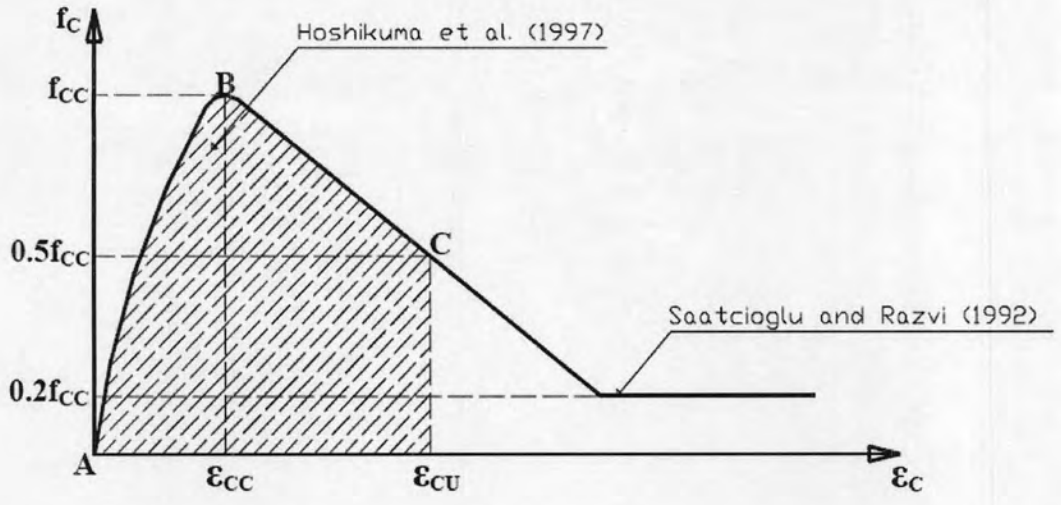

Fig.5.7 Confined concrete model of Hoshikuma *et al.* (1997)

From A-B ($\varepsilon_c \leq \varepsilon_{cc}$): $$f_c = E_c \varepsilon_c \left[1 - \frac{1}{n} \left(\frac{\varepsilon_c}{\varepsilon_{cc}} \right)^{n-1} \right] \quad (5.4)$$

From B-C ($\varepsilon_c > \varepsilon_{cc}$): $$f_c = f_{cc} - E_{des}(\varepsilon_c - \varepsilon_{cc}) \quad (5.5)$$

where

$$n = \frac{E_c \varepsilon_{cc}}{E_c \varepsilon_{cc} - f_{cc}} \quad (5.6a)$$

$$\varepsilon_{cu} = \varepsilon_{cc} + \frac{f_{cc}}{2E_{des}} \quad (5.6b)$$

$$\frac{f_{cc}}{f_{co}} = 1 + 3.8\alpha \frac{\rho_s f_{yh}}{f_{co}} \quad (5.6c)$$

$$\varepsilon_{cc} = 0.002 + 0.033\beta \frac{\rho_s f_{yh}}{f_{co}} \quad (5.6d)$$

$$E_{des} = 11.2 \frac{f_{co}^2}{\rho_s f_{yh}} \quad (5.6e)$$

n = coefficient, and given as equation (2.11a)

f_c = compressive strength of concrete

f_{cc} = ultimate compressive strength of concrete

f_{co} = compressive strength of unconfined concrete

f_{yh} = yield strength of lateral reinforcement

E_c = modulus of elasticity of concrete

E_{des} = deterioration rate of concrete at $\varepsilon_{cc} \leq \varepsilon_c \leq \varepsilon_{cu}$;

ε_{cc} = strain at ultimate strength;

ρ_s = volumetric ratio;

α, β = modification factors depending on the section types such that $\alpha=\beta=1$ for a circular section and $\alpha=0.2$ and $\beta=0.4$ for a rectangular section.

5.2.2 Analysis result of RC section

The moment-curvature relation of the RC section is shown in Figure 5.8. When the curvature of the section reaches 0.0026 m^{-1} and the moment is 0.082 MN.m, crack occurs in concrete. For further state, the tensile steel reaches the strain of 0.003 and yielding occurs. In this state, the curvature is 0.0158m^{-1} and the yield moment is 0.297 MN.m. At the curvature equal to 0.032m^{-1} the section reaches the maximum moment capacity of 0.326 MN.m. The covering concrete spalls out at extreme concrete fiber equal to 0.004. Then the moment capacity continues to drop until the ultimate state. For this state, it is defined at the moment dropped from the maximum moment by 20%. Finally, it could be observed from Figure 5.9 (d) that the failure of the RC section is due to the buckling of the compressive bar under compression. The reduction of the compressive stress in the compressive bar under compression is about is about 28.2%. The curvature ductility could obtain equal to 8. At the same state, the tensile bar is at the beginning of the hardening as shown in Figure 5.9 (c). The core concrete is at the sustained stress as depicted in Figure 5.9 (b). The analysis result is tabulate in Table C.2 in Appendix C.

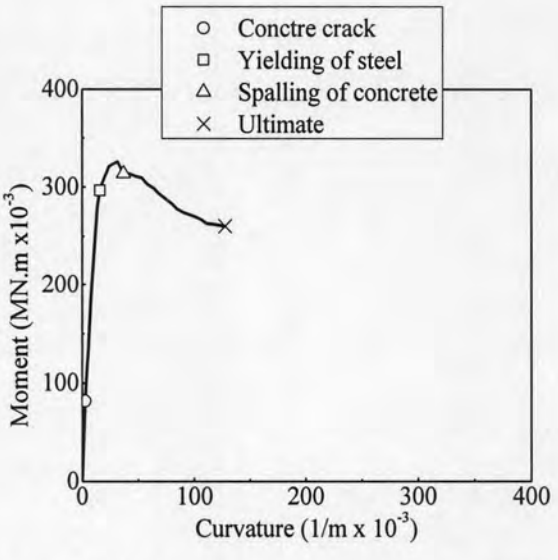

Figure 5.8 Moment-curvature relation of RC section

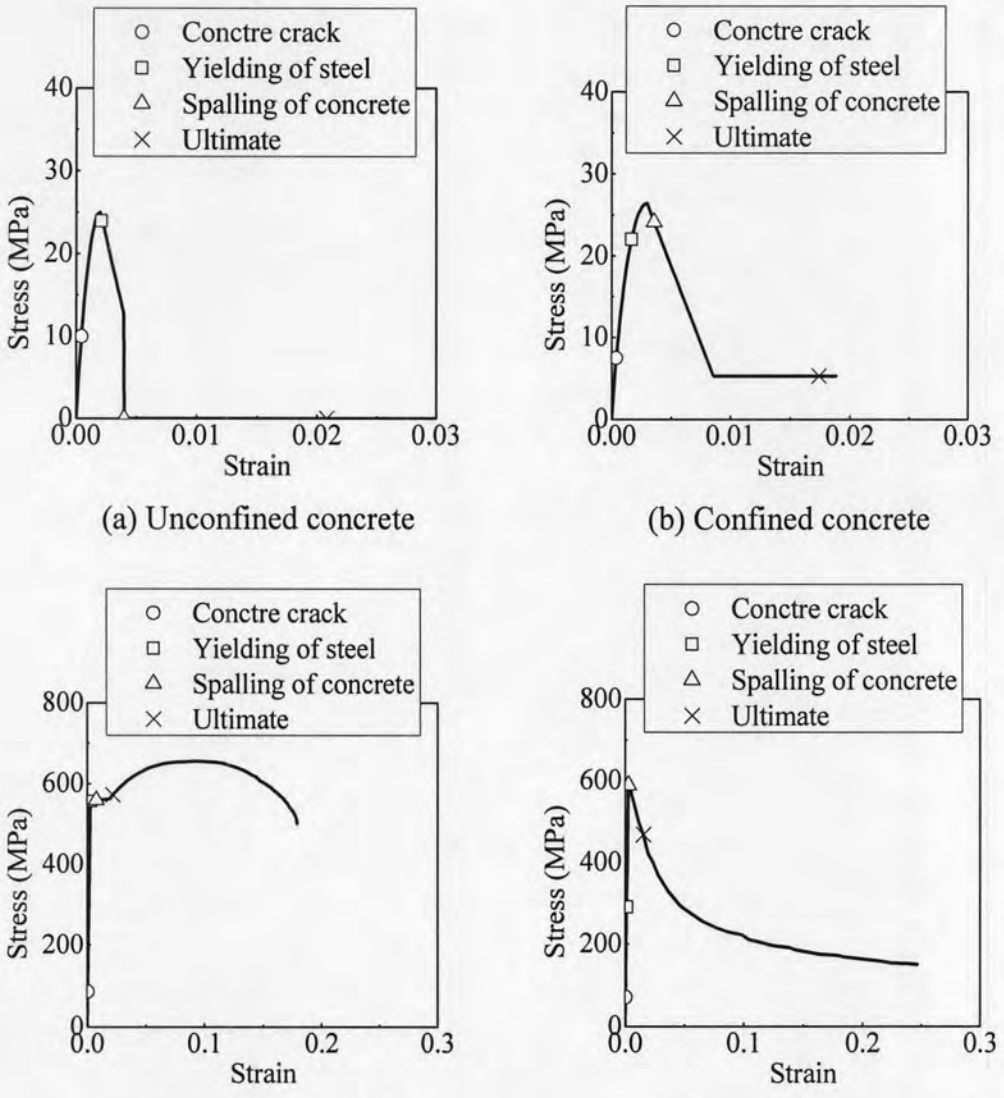

(a) Unconfined concrete

(b) Confined concrete

(c) Steel under tension

(d) Steel under compression

Figure 5.9 Material behavior of RC section at various states of moment-curvature relationship

5.2.3 Analysis result of precast section with mechanical splice T4.0-G54

The moment-curvature relation of the precast section is shown in Figure 5.10. When the curvature of the section reaches 0.0026 m^{-1} and the moment capacity is 0.076 MN.m, in this state the concrete crack occurs. For another state, the tensile splice elongates by the strain 0.0033, the section starts to yield. In this state, the section produces the curvature equal to 0.0158 m^{-1} and the yield moment equal to 0.257 MN.m. Of course, the cover concrete spalls out at extreme concrete fiber equal to 0.004. At curvature equal to 0.047 m^{-1}, the section reaches the maximum moment capacity equal to 0.299 MN.m. Then the moment capacity continues to drop until the

ultimate state, such as 20% from peak moment. The failure of the precast section with mechanical splice T4.0-G54 is also due to the buckling of the splice as shown in Figure 5.11 (d). The reduction of the compressive stress in compressive splice is about 42%. The curvature ductility is equal to 20.05.At the same state, the tensile splice goes beyond the descending branch near the ultimate tensile strain as depicted in Figure 5.11 (c). Figure 5.11 (b) shows that the concrete in the core goes beyond the sustained stress. A summary of the result of the analysis is provided in Table C.3 of Appendix C.

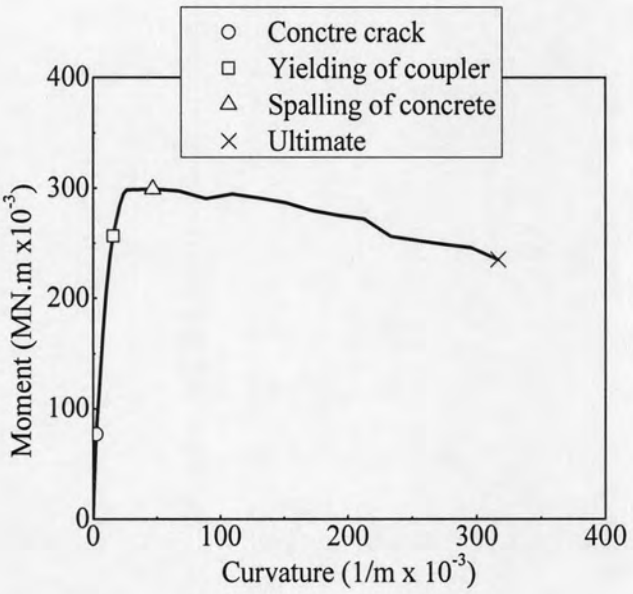

Figure 5.10 Moment-curvature relation of precast section with mechanical splice T4.0-G54

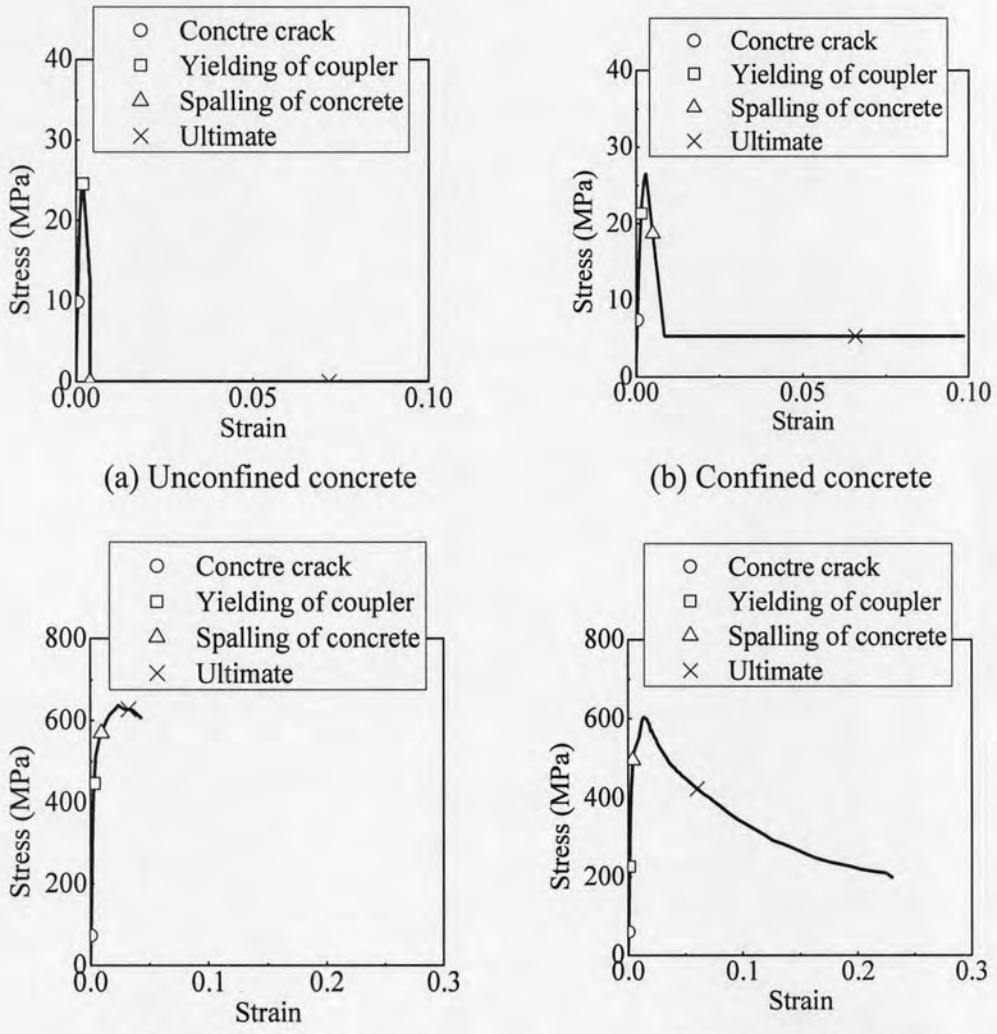

(a) Unconfined concrete

(b) Confined concrete

(c) Tensile Envelope

(d) Compressive Envelope

Figure 5.11 Material behavior of precast section with mechanical splice T4.0-G54 at various states of moment-curvature relationship

5.2.4 Comparison between RC section and pre-cast section with mechanical splices

The moment-curvature relation is shown in Figure 5.12. The curvature ductility of the precast section is about 2.5 times the curvature ductility of the RC section. In addition, the difference of maximum moment capacity is only 9.1%. It should be note that the failure of both columns is due to the buckling of the bars and splices. The splice under compression has more ductility than the bar of the RC section as shown in Figure 5.13 (d).

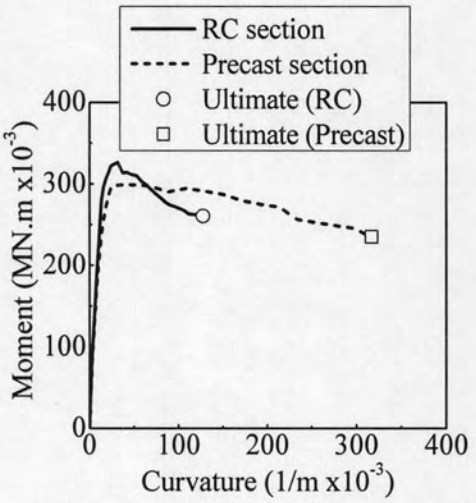

Figure 5.12 Comparison of moment-curvature relation of RC section and precast section with mechanical splice T4.0-G54

Figure 5.14 compares the moment-curvature curves of the RC section and precast sections with mechanical splices for different gap lengths of couplers. The curvature ductilities of precast sections are greater than that of the RC section. The curvature ductility is slightly different for different coupler gap lengths. Table 5.3 summarizes the curvature ductility and maximum moment of RC and precast sections.

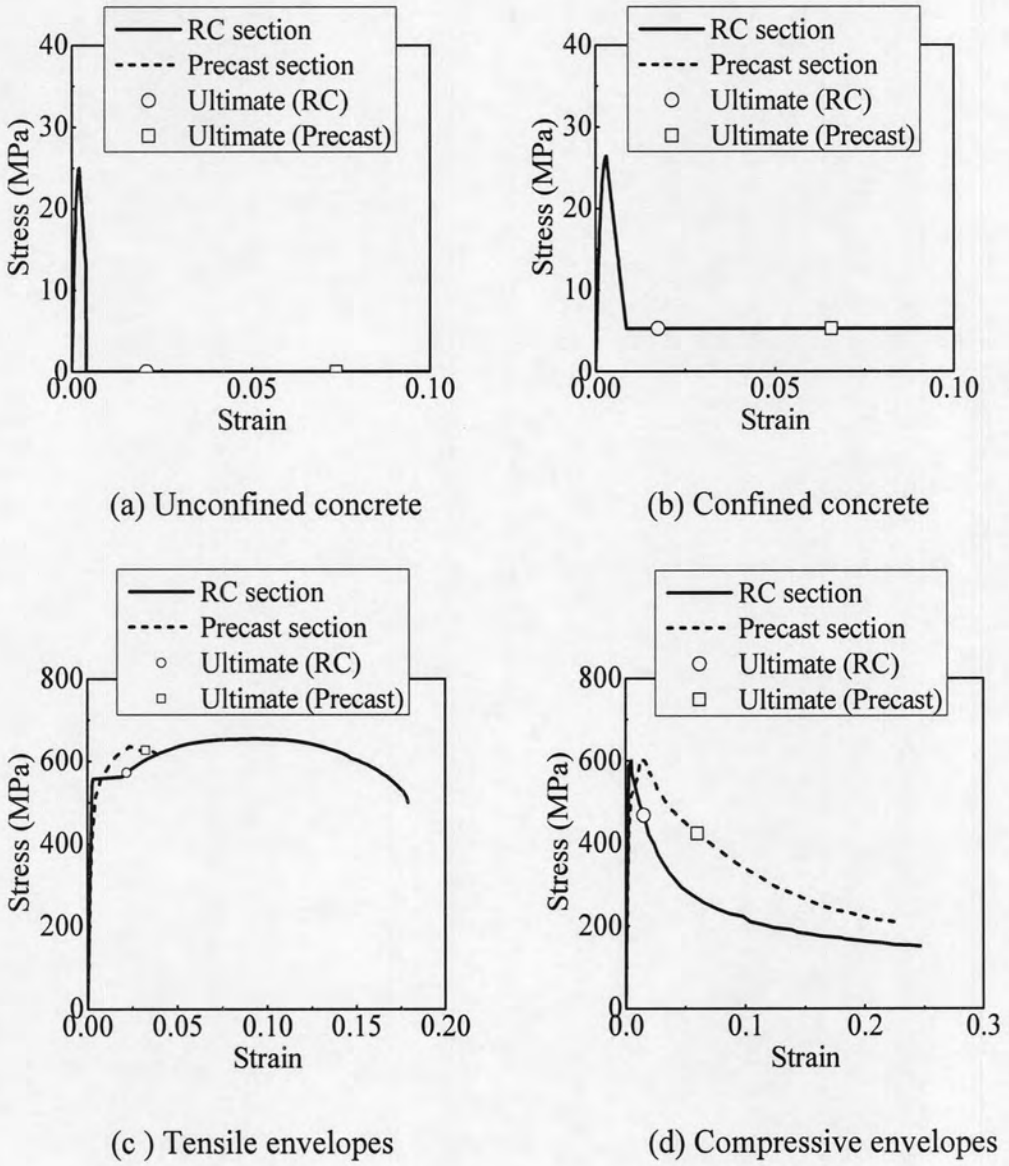

Figure 5.13 Comparison of material behavior of RC column and Pre-cast column with mechanical splice T4.0-G54 at ultimate state (volumetric ratio = 0.77%)

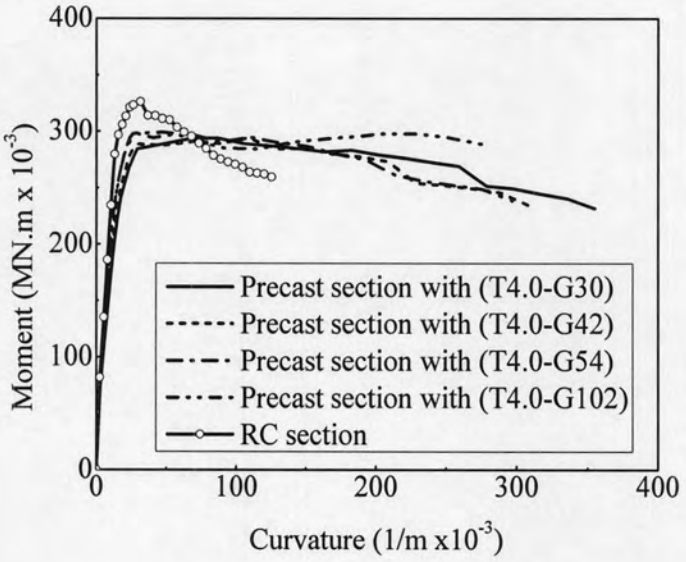

Figure 5.14 Moment-curvature curves of RC section and pre-cast sections with mechanical splices at different coupler gap lengths

Table 5.3 Summary of curvature ductility and maximum moment capacity of RC and precast sections

Splice	Curvature ductility	Maximum moment capacity	Failure mode
		(MN.m x10^{-3})	
T4.0-G30	20.2	294.0	Buckling
T4.0-G42	17.6	294.1	Buckling
T4.0-G54	20.1	299.1	Buckling
T4.0-G102	16.5	298.2	Tensile rupture
Plain bar	8.1	326.1	Buckling

The ultimate state of the columns is controlled by the buckling of the bar and splice. The better performance of the precast sections is due to the buckling behavior of splices.

To check the sensitivity of parameters, the volumetric ratio of lateral reinforcement of the columns is increased from 0.77% to 1.78%. The sections are shown in Figure 5.15. Figure 5.16 shows the moment-curvature relations of RC and precast columns with mechanical splices for different coupler gap lengths. It could be observed that the curvature ductility of the RC section is slightly greater than that of the precast sections. But the maximum moment capacity is almost the same. It should be noted that the bar again fails due to the buckling of the longitudinal reinforcement. On the other hand, the failure of the precast sections is all due to the fracture of the couplers. Table 5.4 summaries the curvature ductility and maximum moment capacity of those columns.

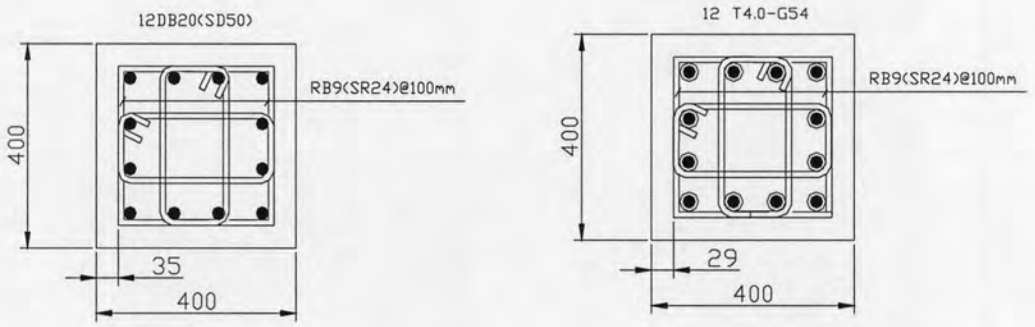

(a) RC section (b) Precast section

Figure 5.15 Configuration of the RC and precast sections with volumetric ratio of lateral reinforcement equal to 1.78%

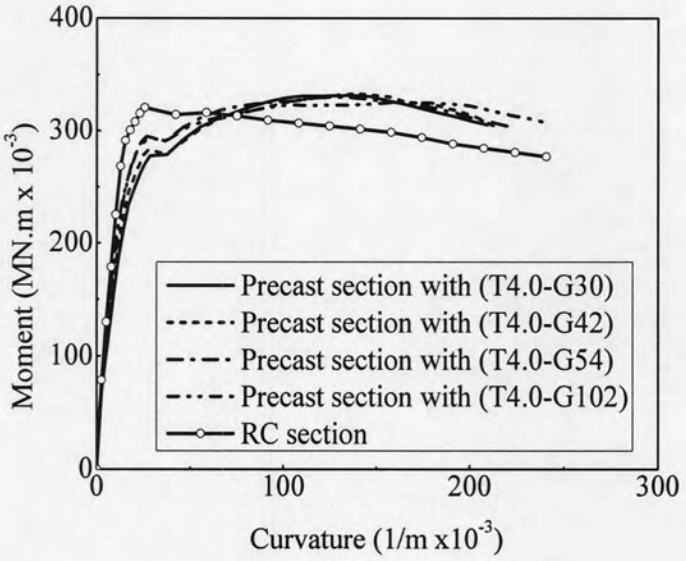

Figure 5.16 Moment-curvature curves of RC section and precast sections with mechanical splices at different coupler gap lengths

Table 5.4: Summary of curvature ductility and maximum moment capacity of RC and precast sections (volumetric ratio = 1.78 %)

Splice	Curvature ductility	Maximum moment capacity	Failure mode
		(MN.m x10^{-3})	
T4.0-G30	9.5	331.4	Tensile rupture
T4.0-G42	10.3	332.9	Tensile rupture
T4.0-G54	11.3	329.8	Tensile rupture
T4.0-G102	15.7	324.9	Tensile rupture
Plain bar	15.6	320.4	Buckling

5.3 Lateral force-displacement analysis

The lateral force-displacement relationship of the RC and pre-cast columns are obtained from the moment-curvature analysis result. The displacement is determined by integrating the curvature over the column height and the lateral force is computed by dividing the moment to the column height, depicted in Figure 5.17. For the RC and precast columns in this study, the height used is equal to 3.0 m. The column is divided into 601 sections, resulting in 600 layers. The thickness of each layer is 0.005 m. The integration of curvatures over the column height is performed to obtained the lateral displacements.

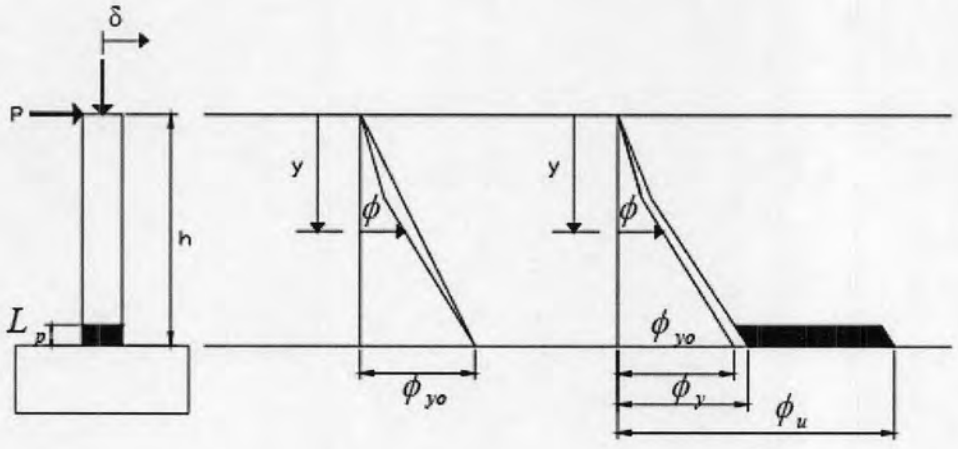

Figure 5.17 Distribution of curvature along column height

From Figure 5.17, the displacement δ at the column top at the elastic state can be estimated from:

$$\delta = \int \phi y dy \approx \sum_{i=1}^{n} (\phi_i y_i + \phi_{i-1} y_{i-1}) \ \Delta y_i / 2 \qquad (5.7)$$

The displacement after the yield moment could be estimated from:

$$\delta = \delta_y + (\phi - \phi_y) L_p \left(h - \frac{L_p}{2} \right) \qquad (5.8)$$

Where, L_p = Plastic hinge length estimated in accordance to the Japanese Design Specifications of Highway Bridges (1996)

$$L_p = \text{Smaller} \begin{Bmatrix} L_p = 0.2h - 0.1D \\ L_p = \dfrac{D}{2} \end{Bmatrix} \quad (5.9)$$

where

h = distance from the pier base to the center of mass;

D = dimension of the cross section in the direction parallel to the direction of an excitation in the analysis;

ϕ_y =yielding curvature;

ϕ = curvature after yielding.

The lateral force-displacement relation for the RC and precast columns can be obtained as shown in Figure 5.18. It is seem that the precast columns with mechanical splices exhibits larger ductility and energy dissipation. Because the improvement of the buckling by the splices. The ductility of the precast column with mechanical splice T4.0-G54 is about 2.1 times the ductility of the RC column. The energy dissipation is 1.88 times the energy dissipation of the RC column. In addition, the maximum force capacity is slightly difference. The difference is approximately 9.1%. Table 5.5 summarizes the displacement ductility and energy dissipation of the RC and precast columns at the same volumetric ratio about 0.77%.

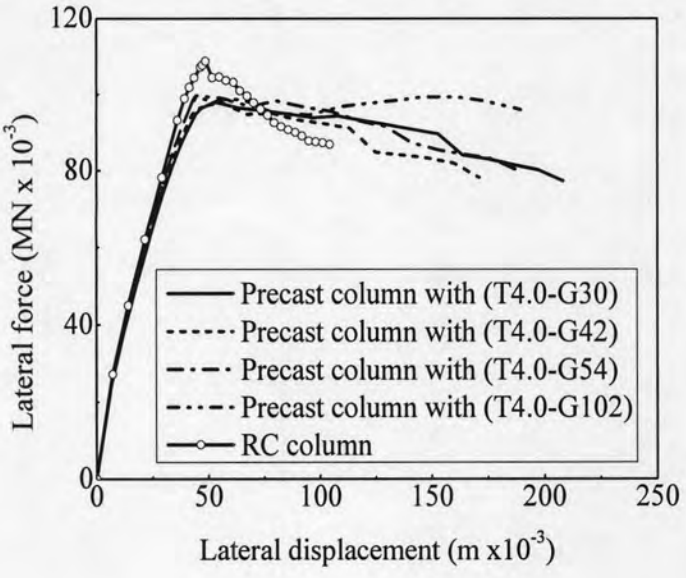

Figure 5.18 Lateral force-displacement curves of RC section and precast sections with mechanical splices at different coupler gap lengths

Table 5.5 Summary of displacement ductility and energy dissipation of RC and precast columns with mechanical splices

Splice	Displacement ductility	Energy dissipation	Failure mode
		(N.m)	
T4.0-G30	6.2	17273	Buckling
T4.0-G42	4.9	13907	Buckling
T4.0-G54	5.5	15924	Buckling
T4.0-G102	5.3	16767	Tensile rupture
Plain bar	2.7	8483	Buckling